International Conference on Mathematics, Computational Methods & Reactor Physics (M&C 2009)
Saratoga Springs, New York, May 3-7, 2009, on CD-ROM, American Nuclear Society, LaGrange Park, IL (2009)

DEVELOPMENT OF PC BASED MONTE CARLO SIMULATIONS FOR THE CALCULATION OF SCANNER-SPECIFIC NORMALIZED ORGAN DOSES FROM CT

Jan T. M. Jansen and Paul C. Shrimpton
Health Protection Agency, Radiation Protection Division, CRCE
Chilton, Didcot, Oxfordshire, OX11 0RQ, United Kingdom
Jan.Jansen@HPA.org.uk; Paul.Shrimpton@ HPA.org.uk

Maria Zankl
Helmholtz Center Munich, German Research Center for Environmental Health (GmbH)
Ingolstädter Landstraße 1, München, Germany
Zankl@helmholtz-muenchen.de

ABSTRACT

This paper discusses the simulation of contemporary computed tomography (CT) scanners using Monte Carlo calculation methods to derive normalized organ doses, which enable hospital physicists to estimate typical organ and effective doses for CT examinations. The hardware used in a small PC-cluster at the Health Protection Agency (HPA) for these calculations is described. Investigations concerning optimization of software, including the radiation transport codes MCNP5 and MCNPX, and the Intel and PGI FORTRAN compilers, are presented in relation to results and calculation speed. Differences in approach for modelling the X-ray source are described and their influences are analysed. Comparisons with previously published calculations at HPA from the early 1990s proved satisfactory for the purposes of quality assurance and are presented in terms of organ dose ratios for whole body exposure and differences in organ location. Influences on normalized effective dose are discussed in relation to choice of cross section library, CT scanner technology (contemporary multi slice versus single slice), definition for effective dose (1990 and 2007 versions) and anthropomorphic phantom (mathematical and voxel). The results illustrate the practical need for the updated scanner-specific dose coefficients presently being calculated at HPA, in order to facilitate improved dosimetry for contemporary CT practice.

Key Words: Computed Tomography, Dosimetry, Monte Carlo

1 INTRODUCTION

In the early 1990's, the National Radiological Protection Board (NRPB), known since 2005 as the Radiation Protection Division of the Health Protection Agency (HPA-RPD), conducted a national survey of computed tomography (CT) practice in the UK [1–3] on the basis of normalized organ doses provided by series of Monte Carlo (MC) calculations modelling 27 common types of CT scanner. In order to promote more widespread dosimetry for patients undergoing CT examinations, these data were made available electronically as software report SR250 [4] in 1993. This included 23 data files each containing 208 sets of normalized doses for 27 organs or regions of a (MIRD) reference adult mathematical phantom [5], corresponding to the irradiation under specific CT conditions of every 5 mm thick transverse slab of the phantom. In 1993, Le Heron [6] developed a personal computer (PC) program to facilitate manipulation of these dose coefficients for the computation of the effective dose for a CT examination. In 2000, the UK CT Evaluation Group (ImPACT) [7] introduced a methodology for matching contemporary scanners to the

published SR250 data sets [4] as part of its widely used dosimetry spreadsheet. Khursheed et al. [8] updated the Monte Carlo calculations at the NRPB by transferring them from a Digital Equipment Corporation (DEC) VAX (Virtual Address eXtension) cluster to a PC and from a home-made FORTRAN program to the general purpose Monte Carlo N-Particle radiation transport code MCNP [9]. In 2002, results were summarized of further normalized organ doses calculated for a family of hermaphrodite (MIRD) phantoms (representing ages 0, 1, 5, 10 and 15 years, as well as adult) for three CT scanner models.

Notwithstanding the continuing wide spread use of report SR250 [4] and its data from the early 1990's, there are compelling reasons why these normalized organ doses are in need of revision. In the last two decades, CT technology has developed significantly with the introduction of multi-row detectors, helical scanning, tube current modulation, increasing resolution, decreasing rotation times and multi x-ray tubes. Furthermore, in 2007 the International Commission on Radiological Protection (ICRP) introduced in Publication 103 [10] an updated definition of effective dose (E_{103}) including new risk and remainder organs compared with that (E_{60}) given in its 1990 recommendations (Publication 60) [11]. Accordingly, normalized doses are required for these additional organs following necessary revision of the previously used anthropomorphic hermaphrodite phantoms. Various voxel phantoms are also now available that mimic the sex specific patient more accurately. Finally, the need for dose assessment in contemporary CT grows ever more important owing to its increasing application in clinical practice and growing importance for population dose.

This article describes the PC-cluster built for these new calculations. As part of quality assurance, a comparison is made with the previous data in SR250 [4] for three CT scanners. Various cross section libraries and methods for implementing the CT X-ray source are described and compared. Comparisons are presented between values of normalized effective dose calculated for both definitions of effective dose, using data from SR250 and new calculations for the exposure of each 1 cm slab of three hermaphrodite mathematical adult phantoms and four sex dependent voxel phantoms.

2 MATERIAL AND METHOD

2.1 Hardware

A dedicated PC cluster has been built for these new calculations, consisting of 11 Supermicro PC-nodes (Super Micro Computer Inc., San Jose, CA) each equipped with two Dual-Core AMD Opteron processors (Advanced Micro Devices, Dresden, Germany) with 8 GB of RAM. Seven of these nodes contain a Supermicro H8DAR-T/E motherboard equipped with two Dual-Core AMD Opteron 265 1.8 GHz processors, whereas four newer nodes contain a Supermicro H8DMR-82 motherboard with two Dual-Core AMD Opteron 2222 3.0 GHz processors. The 10 calculation nodes each have one Seagate Barracuda hard disk with 250 GB and the server node has four 250 GB hard disks connected to an Areca ARC-1110 RAID controller (Areca Technology Corporation, Taipei, Taiwan), operated at RAID Level 5. For back-up purposes, a Sony AIT 2 Turbo tape driver (Sony Corporation, Tokyo, Japan) is connected to the server node. All the nodes are connected with each other through a Netgear Prosafe GS116 Ethernet switch (Netgear Inc., Santa Clara, CA). The server node has an additional Ethernet connection to the outside world. For maintenance purposes, this small PC cluster uses DKVM-8E KVM switches (D-Link Corporation, Fountain Valley, CA) in order to connect a keyboard, monitor and mouse.

2.2 Software

The Fedora Core Linux operating system (Fedora Core, Raleigh, NC) is installed on all the nodes and the batch system OpenPBS (Altair Engineering Inc., Troy, MI) distributes jobs over the various nodes. For radiation transport, the general Monte Carlo N-Particle transport code MCNP is used, as versions MCNP5 1.40 [12], MCNPX 2.5.0 [13] and MCNPX 2.6.0 [14] (Los Alamos National Laboratory, Los Alamos, NM). For testing and timing purposes, evaluation versions of both the PGI (The Portland Group Inc., Lake Oswego, OR) and the Intel (Intel Corporation, Santa Clara, CA) FORTRAN compilers, as recommended by the MCNP developers, have been installed. Various optimization-for-speed flags have been investigated during compilation. The test problem suite supplied with MCNP has been used to check the fidelity of the output generated by the compiled code. A typical problem was created to study timings for the generation of output. This comprised the calculation of organ doses to the Golem voxel phantom from an anterior posterior (AP) beam of ten million photons, each with an energy of 100 keV. Three timings are recognized in the MCNP output file. The $run\text{-}time$ is shown as "computer time in mcrun". The $set\text{-}up\ time$ is computed from "computer time so far in this run" by subtracting the $run\text{-}time$. The $post\text{-}processing\ time$ is computed from "computer time =" by subtracting both the $set\text{-}up$ and $run\text{-}times$.

2.3 Anthropomorphic Phantoms

The adult anthropomorphic phantoms available for our study are the MIRD-like hermaphrodite mathematical phantom used previously, NRPB18+ [8], a modified version to include some of the additional risk and remainder organs, HPA18+ [15], the male voxel phantoms Golem [16] and MAX06 [17], and the female voxel phantoms Laura [18] and FAX06 [17]. For quality assurance purposes, an additional MIRD-like phantom has been created that was based on the hermaphrodite mathematical phantom, NRPB18+ [8], in order to be compatible with that used by Jones [5] to calculate the SR250 data files. This phantom is called NRPB18+DJ. The Monte Carlo calculations have been performed in photon transport only mode and electron equilibrium is assumed for the diagnostic photon energy range, except in relation to bone dosimetry. For this particular case, the distribution of relatively high atomic number cortical bone and relatively low atomic number red bone marrow and endosteal cells, in a mixture with distances in the tens of micrometer range, invalidates the assumption of electron equilibrium and dose enhancement factors have to be applied. Bone surface (or endosteal cell) dose has been calculated as the average dose to the bone mixture, although this is probably an overestimate. Red bone marrow dose has been calculated using bone specific dose enhancement factors from King and Spiers [19], the red bone marrow distribution over various bones given by Cristy [20], the red bone marrow composition given in ICRU Report 44 [21] and mass energy absorption coefficients by Seltzer [22]. In contrast, red bone marrow dose in the SR250 data was calculated using the red bone marrow distribution from ORNL [23], red bone marrow composition of Cristy [23] and mass energy absorption coefficients by Hubbell [24].

2.4 CT Scanners

The three old CT scanners that have been simulated in the new Monte Carlo calculations, as also being present in the SR250 data files, are the General Electric 9800 (General Electric Healthcare, Milwaukee, WI) operated at 120 kV, the Philips Tomoscan LX (Philips Healthcare, Best, The Netherlands) operated at 120 kV and the Siemens Somatom DRH (Siemens Medical Solutions, Forchheim, Germany) operated at 125 kV. The contemporary CT scanner that has been simulated is the Siemens Sensation 16 scanner, operated at 80, 100, 120 and 140 kV tube voltages in both body and head modes.

2.5 X-ray Source Models

Each CT scanner has a rotating X-ray tube delivering the radiation towards the centre of rotation, with a beam collimated both in the plane of rotation, as indicated by the fan angle, and in the Z-axis direction along the rotation axis (perpendicular to the plane of rotation) and dependent on the slice thickness. The X-ray tube spectrum is dependent on the anode material, tube voltage, voltage ripple, the anode angle and the applied homogeneous filter materials and thicknesses, and is generated by the IPEM spectrum processor [25]. A CT-scanner specific bow-tie filter is used to decrease the radiation through the fan borders compared to the fan centre so as to provide a more homogeneous detector response with a patient in the beam. Such details of design and geometry are required to model each CT scanner.

This photon source has a beam that is not symmetric with regard to the azimuthal angle and is rotating around an axis, making it difficult to implement efficiently as a general MCNP defined source. Jones et al. [4] simplified the X-ray source by making the beam parallel in the plane of rotation and implementing bow-tie filters by reducing photon weight (statistical importance) at each fan angle according to the chance of an interaction in the filter. Khursheed et al. [8] also modelled a parallel beam by defining a line source (equal to the thickness of the irradiated slab), and implemented the bow-tie filters in MCNP. This limited the number of simulated line-source and bow-tie filter combinations to 18 for the GE 9800 and Philips LX scanners, and 72 for the Siemens DRH scanner, in order to avoid overlapping filters.

2.5.1 X-ray source model 1

As an initial modelling approach for the present simulations, a user defined $source$ FORTRAN subroutine was implemented. Using the $rdum$ facility, the user defines in the MCNP input file the focus to centre of rotation (COR) distance in cm, R, the focus position along the Z-direction (height of the anthropomorphic phantom) in cm, Z, the slab thickness along the Z-direction on the rotation axis in cm, T, and the start and stop focus positions for a slab in radians relative to the positive X-axis, Φ_{start} and Φ_{stop}, respectively. The particle number, ipt, and the five possible starting cell numbers, '$icl[5]$', are defined by the user in the MCNP input file with the $idum$ facility. The fan angle in radians, ψ, and photon energy in MeV, E, are sampled from the appropriate user defined distributions in the MCNP input file using the MCNP subroutine $smpsrc$. The $source$ FORTRAN subroutine samples the focus angle ϕ as:

$$\phi \;=\; \Phi_{start} + (\Phi_{stop} - \Phi_{start}) \times r \tag{1}$$

where r is a random number between 0 and 1 that is uniformly distributed and resampled whenever it is called. The focus position (x, y, z) is determined as (remember that Z is user defined):

$$(x,\; y,\; z) \;=\; (R \times \cos(\phi),\; R \times \sin(\phi),\; Z) \tag{2}$$

The thickness angle, θ, is defined as the angle between the particle direction as projected onto the rotation plane and the particle direction, and is sampled from a uniform angular distribution:

$$\theta \;=\; \arctan(\frac{T}{2R}) \times (2r - 1) \tag{3}$$

The normalized particle direction (u, v, w) is determined as:

$$(u,\; v,\; w) \;=\; (-\cos(\phi + \psi) \times \cos(\theta),\; -sin(\phi + \psi) \times \cos(\theta),\; \sin(\theta)) \tag{4}$$

The rest of the source definition is trivial, namely a statistical weight for the particle wgt=1, a time of tme=0 in shakes (10^{-8} s), defining the particle by number ipt as supplied by the user in the input file,

specifying jsu=0 to declare that the particle is not on a surface and then defining the starting cell icl with user supplied cell numbers ('$icl[5]$') using MCNP subroutine $namchg$ and testing if the particle is inside this cell with MCNP subroutine $chkcel$. If the particle is in none of the user supplied cells, the MCNP subroutine $expire$ is called to exit the program with an error message. Monte Carlo calculations with this $source$ subroutine do not allow the point or ring detector tally (5) to be used. The disadvantage with this implementation is that the beam cross-section on the COR-axis perpendicular to the focus COR direction is not rectangular anymore, but is slightly bent. For small slice thicknesses, T, this effect is small, but it becomes larger with increasing slice thickness. Therefore a new MCNP $source$ file was defined where the sampling starts in this plane, instead of using angles.

2.5.2 X-ray source model 2

The second approach was therefore to sample from a plane in the user supplied $source$ FORTRAN subroutine using the same user defined variables, except that the slice thickness, T, is changed from a user supplied real value to a distribution that is sampled, and the fan angle, ψ, must be calculated from the variable, s, that is sampled from another user supplied distribution. The latter distribution does contain the attenuation by the bow-tie filter, but not any other attenuation data, since these are included in the source FORTRAN subroutine. A rectangular plane is defined through the COR-axis (Z-axis) perpendicular to the focus COR direction. The shortest distance between the point where the particle hits the rectangular plane without interactions and the Z-axis is the sampled s value in cm. The shortest distance from this intersection point to the focus COR line is the sampled t value in cm. The focus angle in radians, ϕ, is calculated according to Eq. (1). The photon starting position, (x, y, z) is calculated according to Eq. (2). The fan angle ψ is calculated as:

$$\psi \;=\; \arctan(\frac{-s}{R}) \tag{5}$$

The particle starting direction is defined by:

$$(u,\; v,\; w) \;=\; \frac{1}{\sqrt{R^2+s^2+t^2}} \times (-\cos(\phi+\psi) \times \sqrt{R^2+s^2},\; -sin(\phi+\psi) \times \sqrt{R^2+s^2},\; t) \tag{6}$$

The statistical particle weight is:

$$wgt \;=\; (\frac{R}{\sqrt{R^2+s^2+t^2}})^3 \tag{7}$$

This can be explained by the variation in fluence due to the inverse square law with the distance and the angle between the particle direction and the normal to the rectangular plane. The dose in a plane in a parallel beam drops with the cosine of the angle between the beam direction and the normal of the plane. The other source particle variables are determined in the same way as before. The dose distribution in the s, t plane varies independently with the parameters of s and t for this implementation.

2.5.3 X-ray source model 3

The third approach was to separate the calculations into two parts. First, a CT scanner-specific source is simulated by a Monte Carlo calculation with the X-ray tube in a fixed position and the photons reaching a cylinder with a radius of 38 cm and parallel to the Z-axis are written to a phase-space file and killed. A home-made program then reads this phase-space file and randomly chooses an angle between 0 and 2π and adjusts the position and direction of the photons according to a rotation around the Z-axis by this angle. In a second CT scanner-independent simulation, this cylinder is wrapped around the patient or CT dosimetry phantom and the rotated phase-space file is used as the photon source.

2.6 Normalized Doses

For the anthropomorphic phantoms, organ doses per starting photon have been derived. For the standard head and body CT dosimetry phantoms [26], the CT Dose Index (CTDI) [26] expressed in air kerma per starting photon has been derived at the central and four peripheral positions (front, left, rear, and right). For the free-in-air simulation, the axial CTDI per starting photon is derived. The organ doses and CTDIs were normalized by dividing them by the axial CTDI free-in-air. This provides estimates of organ dose per axial CTDI free-in-air and, for the head and body dosimetry phantoms, central and peripheral CTDI per CTDI free-in-air (where the peripheral CTDI is the arithmetic mean of the front, left, rear, and right CTDI values). Values of CTDI measured free-in-air and in the CT dosimetry phantoms are supplied (in mGy per 100 mAs) for a range of scanner models in the ImPACT CT Patient Dosimetry Calculator [7] and corresponding values of CTDI per CTDI free-in-air have been compared to values simulated using MCNPX. Calculations for the CT dosimetry phantoms have been conducted only with the phantom centred on the beam, whereas those for the anthropomorphic phantoms were carried out for a range of beam positions along the Z-axis in one cm increments from below the knee (Z=-50) to the top of the head (Z=95). Doses have been calculated at 146 different locations for each combination of anthropomorphic phantom, CT scanner and operational conditions.

The normalized organ doses for these 146 different locations can be combined into organ doses for a specific CT examination by methods outlined in NRPB SR250 [4]. Effective doses have been calculated using the ICRP tissue weighting factors according to both Publication 60 [11] and Publication 103 [10] in order to allow comparison of different examination protocols or different CT scanners. In calculating the effective dose E_{60}, a mass weighted remainder has been applied, the colon was not mass weighted and no remainder rule was applied in relation to individual slabs, since normally a CT examination will consist of more than one slab. For all anthropomorphic phantoms and CTDI calculations, one hundred million photons have been simulated for each Z-location.

2.7 Quantifying Dose Comparisons with SR250

For the purposes of quality assurance, normalized organ doses have been calculated for each 1 cm thick slab along the Z height for the NRPB18+DJ phantom from -50 cm to 95 cm for the three old CT scanners previously included in Software Report SR250 [4]. The SR250 normalized organ doses were originally presented for the central positions of each 0.5 cm slab from Z= -9.75 to Z=94.25 cm. For ease of comparison, appropriate SR250 slabs have been combined for every 1 cm ranging from Z=-9 to Z=94 cm (central combined slab position) and corrected by the mass energy absorption coefficient of air relative to muscle. Shrimpton et al. [2] derived values of between 0.93 and 0.94 for this ratio and in this paper a fixed value of 0.935 has been used. Whole body normalized organ doses have been derived for both the MCNPX calculations and the SR250 data sets by integrating normalized organ doses over all slabs:

$$D_{Organ,[MCNPX|SR250],Whole\ body} = \sum_{i=-9}^{94} D_{Organ,[MCNPX|SR250],i} \tag{8}$$

Where i is the index for the different slabs of 1 cm thickness and is equal to the central slab height in cm along the anthropomorphic phantom. The ratio of whole body normalized organ doses from MCNPX and SR250 compares the conversion coefficients without regard to any subtle differences in organ position between the data sets.

In order to address this concern, the quantity $\Delta_{Organ,|MCNPX-SR250|,Whole\ body}$ has been defined, as representing the whole body absolute difference in normalized organ doses between the MCNPX and SR250 data sets:

$$\Delta_{Organ,|MCNPX-SR250|,Whole\ body} = \sum_{i=-9}^{94} |D_{Organ,MCNPX,i} - D_{Organ,SR250,i}| \tag{9}$$

This parameter is sensitive to differences not only in the whole body conversion coefficients, but also in normalized organ doses along the height of the phantom. To illustrate this further, consider the following comparisons:

$$\begin{aligned} |\sum_{i=-9}^{94} D_{Organ,MCNPX,i} - \sum_{i=-9}^{94} D_{Organ,SR250,i}| \leq \sum_{i=-9}^{94} |D_{Organ,MCNPX,i} - D_{Organ,SR250,i}| \leq \\ \sum_{i=-9}^{94} D_{Organ,MCNPX,i} + \sum_{i=-9}^{94} D_{Organ,SR250,i} \end{aligned} \tag{10}$$

It should be recognized that absorbed doses, D, are always positive or zero. The first inequality becomes an equality if the signs of all differences $D_{Organ,MCNPX,i} - D_{Organ,SR250,i}$ are the same for all slabs i. This means that the organ location is perfect. The second inequality becomes an equality if the organ dose for MCNPX is non-zero only when the organ dose for SR250 is zero, and vice versa. This means a perfect mismatch in the organ location for the various heights along the phantom. By mathematical rearrangement of Eq. (10) so that the inequality is between 0 and 1, a location match parameter is derived as $\Delta_{Organ,Location,Whole\ body}$, where 0 indicates perfect location and 1 indicates perfect mismatch:

$$\Delta_{Organ,Location,Whole\ body} = \frac{1}{2} + \frac{\sum_{i=-9}^{94} |D_{Organ,MCNPX,i} - D_{Organ,SR250,i}| - \max(\sum_{i=-9}^{94} D_{Organ,MCNPX,i}, \sum_{i=-9}^{94} D_{Organ,SR250,i})}{2 \times \min(\sum_{i=-9}^{94} D_{Organ,MCNPX,i}, \sum_{i=-9}^{94} D_{Organ,SR250,i})} \tag{11}$$

Accordingly, a comparison of the new (MCNPX and NRPB18+DJ anthropomorphic phantom) and old (SR250) normalized organ doses has been performed for the GE 9800, Philips LX and Siemens DRH scanners by plotting the ratio of whole body normalized organ doses from MCNPX and SR250 against the whole body location match parameter $\Delta_{Organ,Location,Whole\ body}$.

3 RESULTS

3.1 System Speed

Installation of the PGI compiler was straight forward, whereas additional libraries needed to be downloaded for the Intel compiler that were not all described in the release notes or manual. When running the test problem suite using compiled code for MCNP5 and MCNPX, the use of optimization-for-speed flags beyond the default level generally resulted in failure, due to unexpected differences in the generated output and these were no longer used. The results of the speed analysis for the test problem involving calculations with the Golem voxel phantom are shown in Table I. The largest difference between the various options amounted to three orders of magnitude in $set\text{-}up\ time$ between MCNPX 2.5.0 and

MCNP5 1.40. Although the $run\text{-}time$ for MCNP5 1.40 was 16% to 20% faster than for MCNPX 2.5.0, this would not be able to offset the delay in set-up until four hundred million particles had been simulated. $Post\text{-}processing\ times$ were insignificant compared with total execution times. On this basis, MCNPX 2.5.0 was chosen as our particle transport code. Intel compiled code was between 17% and 78% faster in $set\text{-}up$ and between 12% and 18% faster in $run\text{-}time$ compared with PGI compiled code. For $post\text{-}processing$, the PGI code was faster than the Intel code, but these times were insignificant compared with the total execution time. Based on these timing data, the Intel FORTRAN compiler was selected. MCNPX version 2.6.0 [14] was subsequently obtained and calculation times were found to be reduced compared with MCNPX 2.5.0, although not significantly so. The data for MCNPX 2.6.0 included in Table I represent combined timings for both the Intel compiled version and the LANL version, since there were no significant differences. In as much as the Monte Carlo photon transport calculations are computationally intensive, one might expect a time reduction of 40% based on processor clock frequency between the standard (1.8 GHz) and new (3.0 GHz) nodes. The observed reductions in $set\text{-}up$, run and $post\text{-}processing\ times$ were 43 $\pm$ 5%, 41 $\pm$ 9% and 8 $\pm$ 38%, respectively. The lower reduction for post-processing could be due in part to the increased time spend on output over computation, although the large uncertainty does not support a strong conclusion. The effects of difference in processor generation, motherboard, etc., can not be differentiated from the processor speed.

Table I. Variation in calculation speed (as $set\text{-}up$, run and $post\text{-}processing\ times$) by version of MCNP, compiler, optimization flag and computing node of the PC Cluster for the simulation of organ doses in Golem from an AP parallel beam comprising ten million photons each of 100 keV.

Node type	MCNP code	F90 / F95 compiler	Optimization flag	$Set\text{-}up\ time$ (min)	$Run\text{-}time$ (min)	$Post\text{-}process\ time$ (min)
Standard	MCNP5 1.40	PGI	fastsse	1621 $\pm$ 16	133 $\pm$ 6	0.01 $\pm$ 0.01
Standard	MCNP5 1.40	Intel	default	909 $\pm$ 52	119 $\pm$ 13	0.02 $\pm$ 0.01
Standard	MCNPX 2.5.0	PGI	default	0.98 $\pm$ 0.01	166.4 $\pm$ 0.7	0.00 $\pm$ 0.01
Standard	MCNPX 2.5.0	Intel	default	0.84 $\pm$ 0.04	141 $\pm$ 12	0.02 $\pm$ 0.01
Standard	MCNPX 2.6.0	Intel	default	0.81 $\pm$ 0.05	126 $\pm$ 18	0.02 $\pm$ 0.01
New	MCNPX 2.6.0	Intel	default	0.46 $\pm$ 0.02	75 $\pm$ 3	0.02 $\pm$ 0.01

Four Monte Carlo calculations can be run simultaneously on each computing node of the cluster, with the exception of those involving the MAX06 and FAX06 anthropomorphic phantoms. These voxel phantoms are so large that such calculations are necessarily limited to two per node, so that 4 GB of RAM are available for execution.

3.2 Cross Section Libraries

MCNPX version 2.5.0 [13] includes four photon cross section libraries and their influence on calculated normalized effective dose is summarized in Fig. 1, where values of E_{60} calculated for each 1 cm slab (without application of the remainder rule) are plotted along the Z-axis of the NRPB18+ phantom, together with the typical statistical uncertainty for each calculation. Differences relative to LIB.04p remain within 5 % for all scanners, all photon libraries and all slabs, with the average over the entire phantom being less than 0.6 %. Library LIB.04p the most recent library is used in all calculations and the older libraries differences are small enough to not investigate them any further.

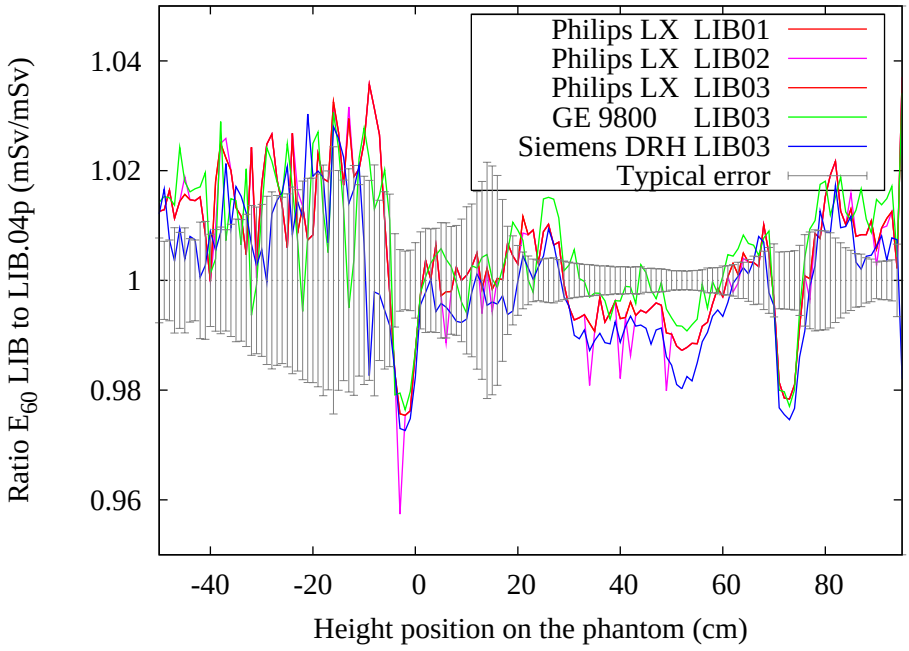

Figure 1. Values of effective dose E_{60} to each 1 cm slab of the NRPB18+ phantom for various photon cross section libraries, relative to data for library LIB04.

3.3 Comparison of X-ray Source Models

Results from the different approaches for modelling the CT X-ray source are summarized in Table II in relation to normalized organ and effective (E_{60}) doses for examination of the whole body using the Philips LX scanner. Relative to data for a line source with continuous rotation (as used in SR250 [4]), discrete rotation of the line source gave organ doses within 3%, whereas the effective dose remained the same. For the more complete approach involving continuous rotation of a point source, normalized organ doses were increased by 2 to 5% and the effective dose was increased by 3%. This is due to an increase in average photon path-length in the phantom arising from the divergence of the X-ray beam in the Z-direction. This effect will become increasingly important for the larger beam thicknesses used in contemporary multi slice CT scanners.

Table II. Comparison of various CT source simulations for the Philips LX scanner as ratios of normalized organ doses per slab and effective doses for whole body exposure of the NRPB18+ anthropomorphic phantom.

Source	Rotation	Minimum organ dose per slab	Maximum organ dose per slab	E_{60} for whole body exposure
Line	Continuous	1	1	1
Line	Discrete	0.98	1.03	1.00
Point	Continuous	1.02	1.05	1.03

3.4 Comparison with SR250

Fig. 2 summarizes the comparison of similar data from the new MCNPX calculations for the NRPB18+DJ anthropomorphic phantom with those published in SR250 [4] in terms of the whole body location match parameter $\Delta_{Organ,Location,Whole\ body}$ and the ratio of whole body normalized organ doses (MCNPX versus SR250) for the following organs: adrenals, brain, breasts, gall bladder, small intestine, lower large intestine, upper large intestine, kidneys, liver, lungs, red marrow, muscle, oesophagus, ovaries, pancreas, skeleton (bone surface), skin, spleen, stomach, testicles, thymus, thyroid, urinary bladder, uterus and whole body.

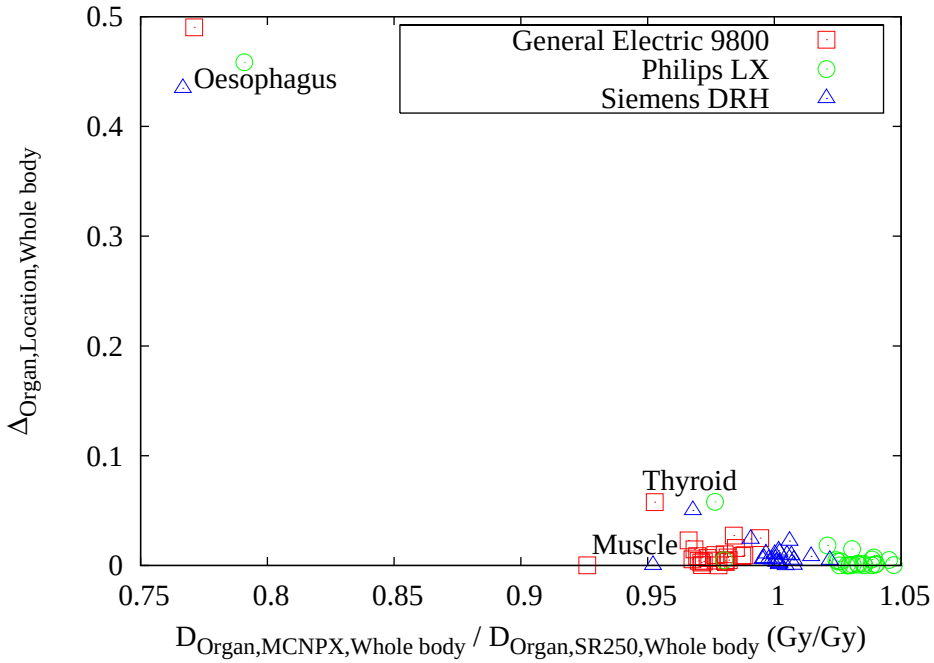

Figure 2. Analysis of differences in dose to 25 organs from MCNPX calculations and SR250 data for three scanner models by location match parameter ($\Delta_{Organ,Location,Whole\ body}$) and ratio for whole body exposure.

For all three scanners, the oesophagus appears to show the largest deviation in both organ dose ratio and location between the data sets, although this reflects the use of thymus dose as a surrogate in the SR250

dose coefficients, since the oesophagus had not been specifically modelled. This discrepancy is also apparent in Fig. 3, which shows normalized doses for selected organs calculated for the Philips LX scanner in relation to each 1 cm slab along the anthropomorphic phantom from Z=-9 to 94 cm. The only other organ for which the difference in whole body normalized organ doses between MCNPX and SR250 exceeds 5% is muscle, and only for the GE 9800 scanner, although the location match is good (Fig. 2). An explanation for this difference might be that muscle is defined as the rest of the body excluding the specified organs and there may be some differences in the modelling of organs between the phantoms used for the MCNPX and SR250 calculations. For the thyroid, the difference in location parameter is about 0.055 for all three scanners and this is due to simplification in modelling this organ in the NRPB18+DJ anthropomorphic phantom. MCNP allows the use of surfaces of first- and second- and fourth-degree elliptical tori, whereas the lobes of the thyroid were originally specified to lie between two concentric cylinders and be formed by a cutting fourth-degree surface that was not an elliptical torus. The next highest difference in location parameter of 0.027 was observed for the ovaries for the GE 9800 scanner, although this was considered insignificant (See Fig. 3). Overall, the reasonable level of agreement between old and new calculations under similar conditions provides confidence in the present dosimetry system using MCNPX.

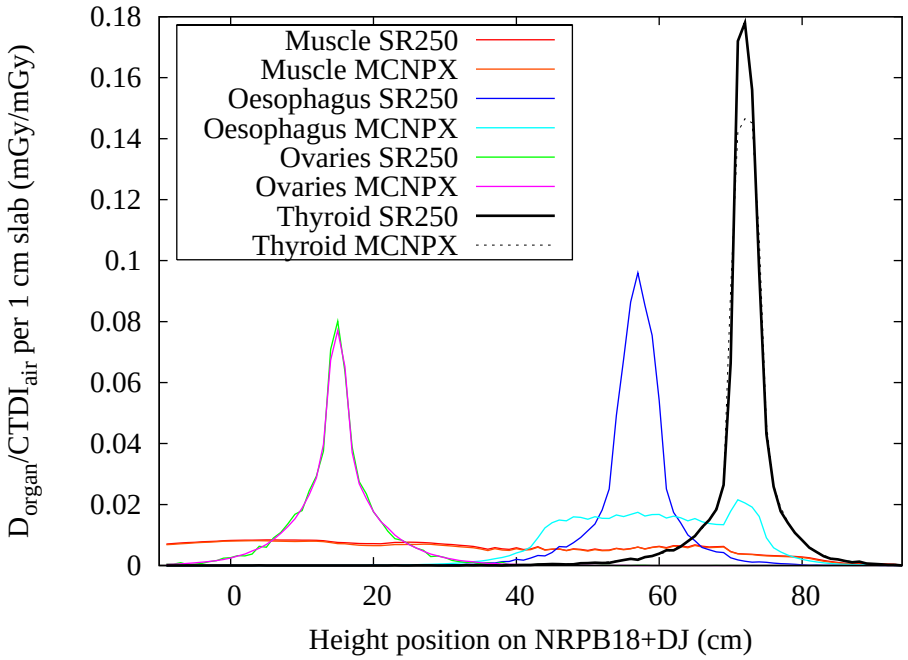

Figure 3. Normalized organ doses versus height along the Z-axis of the phantom NRPB18+DJ for selected organs from the MCNPX and SR250 data sets for the Philips LX scanner.

Comparison of the normalized CTDI doses calculated at the central and peripheral locations in the standard head and body CT dosimetry phantoms with measurements reported by ImPACT [7] also proved satisfactory and is discussed in more detail elsewhere [15].

3.5 Comparing Effective Doses for Different Phantoms

Fig. 4 shows, for the Siemens Sensation 16 CT scanner operated in body mode at 120 kV, the normalized effective dose, $E_{60}/CTDI_{air}$ [11], as a function of height (Z) for the phantoms NRPB18+DJ [5],

NRPB18+ [8], HPA18+ [15], Golem [16], Laura [18], MAX06 [17] and FAX06 [17]. The heights of the voxel phantoms do not exactly match those of the mathematical phantoms, but the phantoms were all aligned at the positions of the gonads. The highest values of normalized effective dose are at the locations of the gonads, for all phantoms. For the hermaphrodite phantoms, the heights of the peaks for the testicles and ovaries are roughly half those for the male or female phantoms, respectively. The thyroid gives rise to a peak for all phantoms, although the Z location is higher for the mathematical phantoms compared with the voxel phantoms, indicating relative differences in modelling. Normalized effective doses, E_{60}, vary due to the sex of the phantom in the region of the testicles, ovaries, uterus and breasts. Agreement is closest between the three MIRD-like phantoms, with larger differences being apparent for the voxel phantoms. This clearly indicates the need for reference phantoms in order to help standardize reported doses, as hopefully will be provided by the ICRP [27] Reference Male and Female Computational Phantoms, RMCP and RFCP, respectively. Whereas report SR250 [4] did not specifically include data for the Siemens Sensation 16, this contemporary scanner has been matched by ImPACT [7] to an existing data set (in this case for the Philips Tomoscan 310 operated at 120 kV with setting GE 3 and added copper filtration) and these data are also included in Fig. 4.

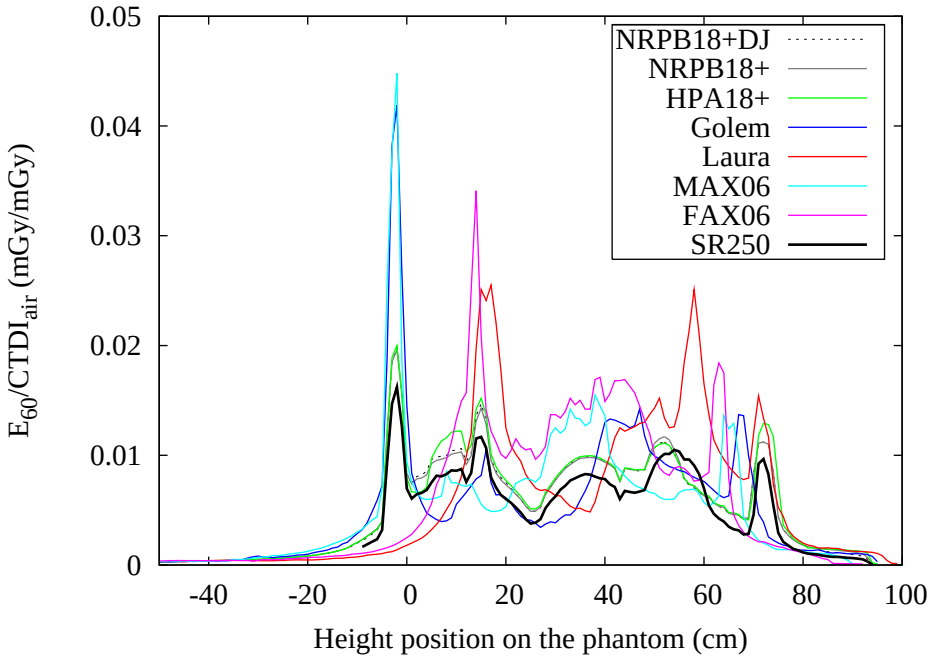

Figure 4. Normalized effective dose, $E_{60}/CTDI_{air}$, for each 1 cm slab of various anthropomorphic phantoms calculated for the Siemens Sensation 16 scanner operated in body mode at 120 kV.

Fig. 5 shows similar data for the Siemens Sensation 16 in relation to values of the normalized effective dose, $E_{103}/CTDI_{air}$ [10], using surrogates for risk or remainder organs not otherwise available, as described by Jansen et al. [15]. Peaks for the testicles and ovaries are still apparent and dependent on the sex (male, female or hermaphrodite) of the phantom, although they no longer represent the highest values owing to the decrease in the tissue weighting factor for the gonads (from 0.20 for E_{60} to 0.08 for E_{103}). For the MIRD phantoms, effective doses for the HPA18+ phantom are clearly different to those for the NRPB18+ and NRPB18+DJ phantoms, and also the SR250 matched data, for the neck and head region. This illustrates limitations in the use of surrogate tissues for risk and remainder organs. The effective doses from the SR250 matched data are below those specifically calculated for the Sensation 16 using the NRPB18+DJ and NRPB18+ phantoms, indicating limitations in the broad method developed by ImPACT

to match contemporary scanners to those modelled in report SR250, thus reinforcing the need for the further scanner-specific simulations that are underway at HPA-RPD.

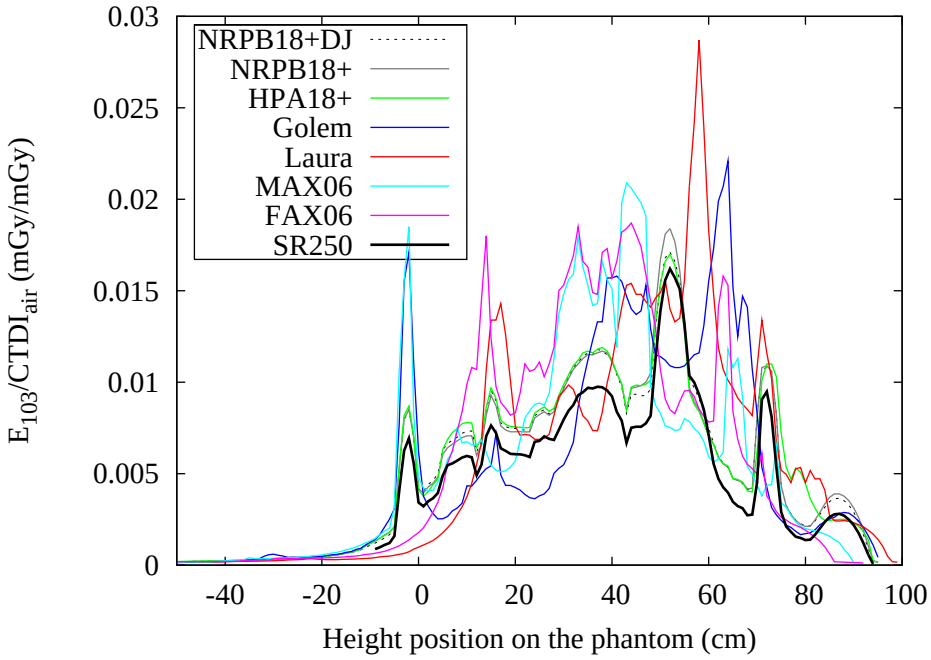

Figure 5. Normalized effective dose, $E_{103}/CTDI_{air}$, for each 1 cm slab of various anthropomorphic phantoms calculated for the Siemens Sensation 16 scanner operated in body mode at 120 kV.

4 CONCLUSIONS

A dedicated PC cluster has been commissioned and optimized for Monte Carlo calculations to derive normalized organ doses for specific X-ray CT scanners. The code MCNPX with the Intel FORTRAN compiler proved most suitable for large voxel phantom calculations. The rotating X-ray source was best modelled in a two-stage calculation, involving the derivation of a phase-space file for a static scanner-specific source, followed by random rotation of the particles in this file around an anthropomorphic or dosimetry phantom. Previously published results [4] for normalized organ doses to a MIRD anthropomorphic phantom (NRPB18+DJ) for simulated whole body exposure with the GE 9800, Philips LX and Siemens DRH scanners were satisfactorily reproduced, with minor differences in relation to the oesophagus, thyroid and muscle being well understood. Calculations for the updated adult MIRD phantoms, NRPB18+ [8] and HPA18+ [15], demonstrate that the use of surrogate risk and remainder organs in the calculation of the 2007 definition of effective dose E_{103} leads to substantial differences in the head and neck region. Further simulations for two male, Golem [16] and MAX06 [17], and two female, Laura [18] and FAX06 [17], voxel phantoms have demonstrated the significant influence of choice of anthropomorphic phantom on both organ and effective doses, and the need for standard reference phantoms (as being developed by ICRP [27]) in order to facilitate comparison of doses between CT studies. Recent changes in the definition of effective dose (from E_{60} to E_{103}) lead to large differences in normalized effective dose per 1 cm slab, although these will be reduced when averaging over the larger scan lengths typically used for CT examinations. Specific calculations for the Siemens Sensation 16 multi slice scanner have illustrated limitations in the method developed by ImPACT [7] for matching contemporary scanners to existing data sets for older scanners previously modelled in report SR250 [4]. There is a need to update

these data in order to facilitate dose assessment for contemporary CT, in light of all subsequent developments, and series of Monte Carlo calculations are in progress at HPA-RPD in collaboration with major CT manufacturers.

ACKNOWLEDGEMENTS

The authors wish to express their thanks to Prof. Dr. Kramer for the use of his phantoms, MAX06 and FAX06 [17], fruitful discussions about bone dosimetry and comparison of organ doses in an AP irradiation field.

REFERENCES

[1] P. C. Shrimpton, D. Hart, M. C. Hillier, B. F. Wall, and K. Faulkner, *Survey of CT Practice in the UK. Part 1: Aspects of Examination Frequency and Quality Assurance*, National Radiological Protection Board, Chilton, UK, (1991).

[2] P. C. Shrimpton, D. G. Jones, M. C. Hillier, B. F. Wall, J. C. Le Heron, and K. Faulkner, *Survey of CT Practice in the UK. Part 2: Dosimetric Aspects*, National Radiological Protection Board, Chilton, UK, (1991).

[3] D. G. Jones and P. C. Shrimpton, *Survey of CT Practice in the UK. Part 3: Normalised Organ Doses Calculated using Monte Carlo Techniques*, National Radiological Protection Board, Chilton, UK, (1991).

[4] D. G. Jones and P. C. Shrimpton, *Software Normalised Organ Doses for X-ray Computed Tomography Calculated using Monte Carlo Techniques*, National Radiological Protection Board, Chilton, UK, (1993).

[5] D. G. Jones and B. F. Wall, *Organ Doses from Medical X-ray Examinations Calculated Using Monte Carlo Techniques*, National Radiological Protection Board, Chilton, UK, (1985).

[6] J. C. Le Heron, *CTDOSE: A User's Guide*, National Radiation Laboratory, Christchurch, New Zealand, (1993).

[7] M. Lewis, *CT Dosimetry: ImPACT spreadsheet for calculating organ and effective doses from CT*, St. George's Hospital, London, UK, (2004).

[8] A. Khursheed, M. C. Hillier, P. C. Shrimpton, and B. F. Wall, "Influence of patient age on normalized effective doses calculated for CT examinations," *Br J Radiol*, **75**, pp. 819–830, (2002).

[9] J. F. Briesmeister, *MCNP — A General Monte Carlo N-Particle Transport Code, Version 4B*, Los Alamos National Laboratory, Los Alamos, NM, (1997).

[10] International Commission on Radiological Protection, "The 2007 Recommendations of the International Commission on Radiological Protection. ICRP Publication 103," *Ann ICRP*, **37**, pp. 1–332, (2007).

[11] International Commission on Radiological Protection, "1990 Recommendations of the International Commission on Radiological Protection. ICRP Publication 60," *Ann ICRP*, **21**, pp. 1–201, (1991).

[12] T. E. Booth, F. B. Brown, J. S. Bull, R. A. Forster, J. T. Goorley, H. G. Hughes, R. D. Mosteller, R. E. Prael, A. Sood, J. E. Sweezy, A. Zukaitis, M. Boggs, and R. Martz, *MCNP — A General Monte Carlo N-Particle Transport Code, Version 5*, Los Alamos National Laboratory, Los Alamos, NM, (2003).

[13] D. B. Pelowitz, *MCNPX User's Manual, Version 2.5.0*, Los Alamos National Laboratory, Los Alamos, NM, (2005).

[14] D. B. Pelowitz, *MCNPX User's Manual, Version 2.6.0*, Los Alamos National Laboratory, Los Alamos, NM, (2008).

[15] J. T. M. Jansen, P. C. Shrimpton, and M. Zankl, "Development of Monte Carlo simulations to provide contemporary CT Scanner-specific Dose Coefficients," To be submitted to Phys Med Biol, (2009).

[16] M. Zankl and A. Wittmann, "The adult male voxel model "Golem" segmented from whole-body CT patient data," *Radiat Environ Biophys*, **40**, pp. 153–162, (2001).

[17] R. Kramer, H. J. Khoury, J. W. Vieira, and V. J. Lima, "MAX06 and FAX06: update of two adult human phantoms for radiation protection dosimetry," *Phys Med Biol*, **51**, pp. 3331–3346, (2006).

[18] M. Zankl, J. Becker, U. Fill, N. Petoussi-Henß, and K. F. Eckerman, "GSF male and female adult voxel models representing ICRP reference man - the present status," *Proceedings of The Monte Carlo Method: Versatility Unbounded in a Dynamic Computing World*, Chattanooga, TN, (2005).

[19] S. D. King and F. W. Spiers, "Photoelectron enhancement of the absorbed dose from X rays to human bone marrow: experimental and theoretical studies," *Br J Radiol*, **58**, pp. 345–356, (1985).

[20] M. Cristy, "Active bone marrow distribution as a function of age in humans," *Phys Med Biol*, **26**, pp. 389–400, (1981).

[21] International Commission on Radiation Units and Measurements, *Tissue Substitutes in Radiation Dosimetry and Measurement. ICRU Report 44*, International Commission on Radiation Units and Measurements, Bethesda, MA, (1989).

[22] S. M. Seltzer, "Calculation of photon mass energy-transfer and mass energy-absorption coefficients," *Radiat Res*, **136**, pp. 147–170, (1993).

[23] M. Cristy, *Mathematical phantoms representing children of various ages for use in estimates of internal dose. NUREG/CR-1159, ORNL/NUREG/TM-367*, Oak Ridge National Laboratory, Oak Ridge, TN, (1980).

[24] J. H. Hubbell, "Photon mass attenuation and energy-absorption coefficients from 1 keV to 20 MeV," *Int J Appl Radiat Isot*, **33**, pp. 1269–90, (1982).

[25] K. Cranley, B. J. Gilmore, G. W. A. Fogarty, and L. Desponds, *Catalogue of Diagnostic X-ray Spectra and Other Data*, Institute of Physics and Engineering in Medicine, York, UK, (1997).

[26] International Electrotechnical Commission, *Medical electrical equipment - Part 2-44: Particular requirements for the safety of X-ray equipment for computed tomography - Amendment 1 - Corrigendum 1*, International Electrotechnical Commission, Geneva, Swiss, (2006).

[27] International Commission on Radiological Protection, "The ICRP Reference Computational Phantoms of the Adult Male and Female," http://www.icrp.org/docs/Reference_phantom_summary_for_web.doc, (2008).